

A detailed comparison of mouse and human cardiac development

Anita Krishnan^{1,2}, Rajeev Samtani^{1,3}, Preeti Dhanantwari⁴, Elaine Lee^{1,5}, Shigehito Yamada⁶, Kohei Shiota⁶, Mary T. Donofrio², Linda Leatherbury^{1,2} and Cecilia W. Lo^{1,7}

BACKGROUND: Mouse mutants are used to model human congenital cardiovascular disease. Few studies exist comparing normal cardiovascular development in mice vs. humans. We carried out a systematic comparative analysis of mouse and human fetal cardiovascular development.

METHODS: Episcopic fluorescence image capture (EFIC) was performed on 66 wild-type mouse embryos from embryonic day (E) 9.5 to birth; 2-dimensional and 3-dimensional datasets were compared with EFIC and magnetic resonance images from a study of 52 human fetuses (Carnegie stage 13–23).

RESULTS: Time course of atrial, ventricular, and outflow septation were outlined and followed a similar sequence in both species. Bilateral venae cavae and prominent atrial appendages were seen in the mouse fetus; in human fetuses, atrial appendages were small, and a single right superior vena cava was present. In contrast to humans with separate pulmonary vein orifices, a pulmonary venous confluence with one orifice enters the left atrium in mice.

CONCLUSION: The cardiac developmental sequences observed in mouse and human fetuses are comparable, with minor differences in atrial and venous morphology. These comparisons of mouse and human cardiac development strongly support that mouse morphogenesis is a good model for human development.

Congenital heart defects occur in an estimated 8/1,000 live births (1). This brings with it a tremendous societal impact due to high morbidity, mortality, and associated healthcare costs. Although palliative procedures are now available for most forms of congenital heart disease, we do not fully understand the underlying mechanisms of most abnormalities of cardiac development in the human fetus. Learning more about these causative mechanisms will allow us to develop sophisticated and successful therapies to prevent abnormalities. This will require clinicians and researchers to have a basic understanding of normal development in early gestation. Much of the research in the area of cardiac development must be

conducted using mammalian models like the mouse, because of obvious ethical and technical roadblocks to any form of study in the human fetus. Molecular studies in mouse models are yielding insight into the mechanisms of congenital valvular disease; however, it remains to be seen whether these studies will translate to insight about congenital heart disease in humans (2,3). Surprisingly, no reference exists in the literature where key morphogenetic events in the human and mouse are laid out side-by-side for developmental biologists who perform these studies, as well as clinicians who seek to understand basic cardiac development.

Normal development of the mouse and human fetal heart has been described (4–10), though to our knowledge no comprehensive study has compared mouse to human development. A few studies have examined the timeline of cardiac development in mice vs. humans (11,12) or broadly examined species-specific variations in cardiac development (13); however, to our knowledge, no study has comprehensively and systematically compared mouse and human fetal cardiac development using the same 3-dimensional (3D) imaging techniques of magnetic resonance imaging (MRI) or episcopic fluorescence image capture (EFIC) for both species. Rather, the majority of studies have made assumptions based on interpretation of reconstructed 3D models from stacks of 2-dimensional (2D) histologic slides. Other researchers described the timeline of mouse development using scanning electron microscopy, however left questions regarding ventricular and outflow septation (6,7).

We and others have described the potential for EFIC to overcome the limitations of other imaging modalities (14,15). Prior work by Rosenthal *et al.* (14) and Dhanantwari *et al.* (16) used EFIC to capture critical developmental events in mouse and human fetal hearts, respectively, and comprehensive online atlases have been created for both species. We aim to compare morphogenesis between the mouse and human and present this information in an easily accessible format. This information will serve as a tool for developmental biologists and clinicians studying fetal cardiac development in the first trimester.

The first two authors contributed equally to this work.

¹Laboratory of Developmental Biology, National Heart, Lung, and Blood Institute, National Institutes of Health, Bethesda, Maryland; ²Children's National Heart Institute, Children's National Medical Center, Washington, DC; ³George Washington University Medical School, Washington, DC; ⁴Division of Pediatric Cardiology, Schneider Children's Hospital, New Hyde Park, New York; ⁵Uniformed Services University of the Health Sciences, Bethesda, Maryland; ⁶Congenital Anomaly Research Center, Kyoto University Graduate School of Medicine, Kyoto, Japan; ⁷Department of Developmental Biology, University of Pittsburgh School of Medicine, Pittsburgh, Pennsylvania. Correspondence: Anita Krishnan (akrishna@childrensnational.org)

Received 22 November 2013; accepted 29 May 2014; advance online publication 24 September 2014. doi:10.1038/pr.2014.128

RESULTS

We reviewed a total of 66 mouse embryos and 52 human embryos. Structures of the atrial septum, ventricular septum, and outflow septum were clearly visualized by EFIC imaging for the mouse and by EFIC and MRI for the human. An overview of comparative developmental stages in the mouse and human is provided in [Table 1](#), and the key differences in morphogenesis are outlined in [Table 2](#). A list of the number of specimens reviewed at each developmental stage is provided in [Supplementary Table S1](#) online. The stages at which key anatomic structures can be identified are compared in [Figures 1](#) and [2](#).

Atrial Septation

Atrial septation in mice occurred over embryonic day (E) 10.5–E13.5; in human fetuses, this was comparable to Carnegie stage (CS) 14–18 or estimated gestational age (EGA) 6 6/7–8 wk. The primary atrial septum, a left sided structure, develops from the superior aspect of the common atrium between the systemic and pulmonary vein orifices. It was first noted at E10.5 in the mouse and CS 14 (6 6/7 wk EGA) in the human ([Figure 3e](#)). At the inferior end of the primary septum is a mesenchymal cap, which could be seen merging with the superior endocardial cushion, and indicated by the arrowhead in [Figure 3e](#). The vestibular spine, a mesenchymal structure,

Table 1. Parallel stages of cardiovascular development in mouse and human

Mouse developmental stage (E)	Human Carnegie stage	Human EGA (weeks)	Major morphogenetic events
9.5–10.5	13–17	6 4/7–7 5/7	Cardiac loop
11.5	15–16	7 1/7–7 3/7	Atrial septation, muscular interventricular septum formation, early outflow septation
12.5	17–18	7 5/7–8	Atrial septation, outlet ventricular septum formation, beginning of semilunar valve formation
13.5	19–21	8 2/7–8 6/7	Completion of membranous/inlet ventricular septum formation
14.5	22	9 1/7	All definitive major cardiac structures identifiable
15.5–17.5	23	23	Progressive myocardial compaction, AV and semilunar valve refinement
17.5 to birth	No comparable stage	No comparable stage	Continued myocardial compaction, semilunar valve refinement

AV, atrioventricular; E, days postconception; EGA, estimated gestational age.

Table 2. Major cardiac morphogenetic differences between mouse and human

Presence of bilateral superior venae cavae in mouse; single right-sided SVC in human
Failure of tricuspid valve septal leaflet to delaminate <i>in utero</i> in mouse
Size of atrioventricular septum is thick and muscular in mouse, thin and fibrous in human
No differences in trabeculations in right and left ventricle of mouse seen by EFIC
Absence of identifiable moderator band in the mouse
Single pulmonary venous orifice in mouse; two to four pulmonary venous orifices in human
Atrial appendages in mouse appear more prominent than in human; right different from left atrial appendages cannot be reliably distinguished from our imaging

EFIC, episcopic fluorescence image capture; SVC, superior vena cava.

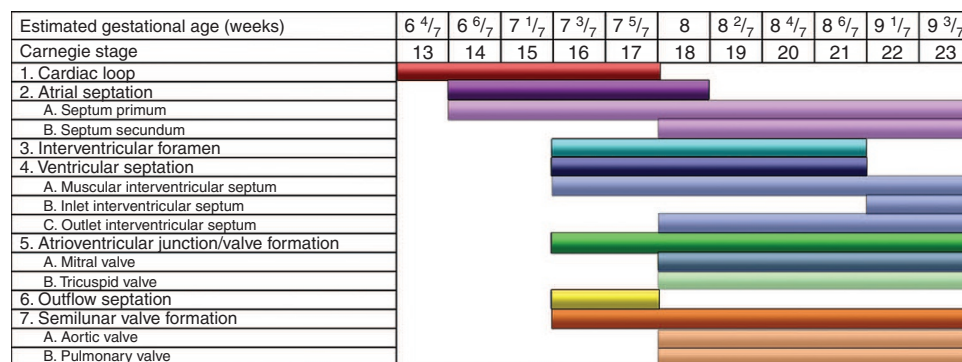


Figure 1. Stages of development in the human heart are outlined. Reprinted from ref. (16).

begins to grow from the posterior aspect of mediastinum, rightward of the pulmonary vein orifice. The vestibular spine was present at stage E11.5 in the mouse. At this stage, septum secundum was noted as well. The ostium primum had not yet closed at this stage. Image quality of the atrial septum from the E10.5 and E11.5 mouse specimens was not of high enough quality for publication in the figures, but these structures are illustrated in the human in [Figure 3e](#). The mesenchymal cap, vestibular spine, and superior and inferior cushions eventually fuse, effectively eliminating the ostium primum ([Figure 3a,e](#)). The mesenchymal tissue becomes muscularized (9) and is the structure known postnatally as septum primum. A second opening, the ostium secundum, develops from dissolution of

the superior aspect of the primary atrial septum and is termed the foramen ovale by fetal echocardiographers. Septum secundum forms from a tissue fold from the posterior portion of the atrium to right of the pulmonary vein orifice (9).

Ventricular Septation

The process of ventricular septation spans E11.5–E13.5 in mice, and EGA 7 3/7–9 1/7 wk (CS 16–22) in human fetuses. The cardiac loop, with undivided right and left ventricles is illustrated in [Figure 3a](#) for the mouse and [Figure 3e](#) for the human, although in some E10.5 specimens, a tiny muscular septum was present. The beginning of true separation of left and right ventricles was seen as early as E11.5 in mouse and CS 16 (EGA 7 3/7 wk) in humans with early signs of formation of the muscular interventricular septum. There is rapid progression of the muscular interventricular septum from CS 16–18 ([Figure 3f](#)) in the human and E11.5–E12.5 ([Figure 3b](#)) in the mouse, although a significant interventricular communication still exists.

Fused cushions originating from the right ventricle begin to rotate at human CS 16 (EGA 7 3/7 wk) and mouse stage E11.5. The outflow cushions fuse with the muscular septum and the atrioventricular cushions in the last step of ventricular septation. This results in closure of a portion of the interventricular foramen, an area termed by clinicians as comprising part of the “membranous” and “inlet” ventricular septae, although work by embryologists has suggested that the inlet septum is not a discrete structure. This occurs at E13.5 ([Figure 3d](#)) in the mouse and CS 22 (EGA 9 1/7 wk; [Figure 3h](#)) in the

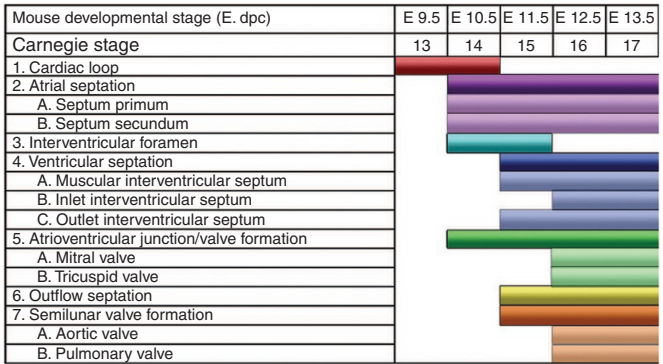


Figure 2. Stages of development in the mouse heart are outlined. Reprinted from ref. (16). Copyright 2009 American Heart Association.

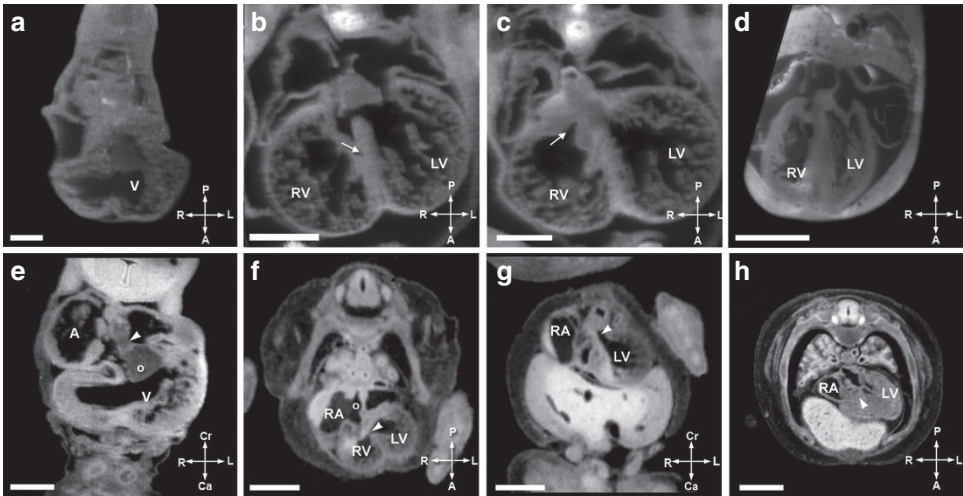


Figure 3. Comparative ventricular septation. (a–d) Ventricular septation in the mouse and (e–h) ventricular septation in the human. Panels a and e show the cardiac loop in the mouse and human, respectively. The arrowhead in e illustrates the atrial spine fusing with the inferior cushion (o). The muscular interventricular septum begins to develop at 7 3/7 wk (CS 16) in the human and E10.5 in the mouse. Note the rapid progression of the muscular interventricular septum by E12.5 (b) in the mouse and EGA 8 wk (CS 18) (f) in the human. At this stage, the outlet septum, indicated by the arrowhead in g, is closed (c, mouse; g, human), but the interventricular foramen (arrowhead in f) comprises a small portion of what is clinically termed the membranous and inlet ventricular septum. Panels d (mouse, E13.5) and h (human, EGA 9 1/7 wk, CS 22) show closure of the final portion of the interventricular foramen (arrowhead). (a) Mouse heart at E10.5. Scale bar = 250 μm. V, ventricle. (b) Mouse heart at E12.5. Scale bar = 550 μm. The arrowhead indicates the muscular interventricular septum. LV, left ventricle; RV, right ventricle. (c) Mouse heart at E12.5. Scale bar = 450 μm. The arrowhead indicates the outlet ventricular septum. (d) Mouse heart at E13.5. Scale bar = 600 μm. (e) Human heart at EGA 6 6/7 wk (CS 14). Scale bar = 500 μm. The “o” symbol indicates the endocardial cushion, and arrowhead shows the mesenchymal cap. A, atrium. (f) Human heart at EGA 8 (CS 18). Scale bar = 1,500 μm. The arrowhead indicates the interventricular foramen, and “o” symbol shows the septum primum. RA, right atrium. (g) Human heart at EGA 8 (CS 18). Scale bar = 1,500 μm. The arrowhead shows the outlet ventricular septum. (h) Human heart at EGA 9 1/7 wk (CS 22). Scale bar = 2,000 μm. The arrowhead shows the closed interventricular foramen. Panels e–h are reprinted from ref. (16). Copyright 2009 American Heart Association. CS, Carnegie stage; E, embryonic day; EGA, estimated gestational age.

human. The true membranous septum develops from conversion of muscular tissue in the proximal outflow cushions to fibrous tissue. At this point, in the human but not mouse, the septal leaflet of the tricuspid valve delaminates (9,16). **Figure 4** shows that the septal leaflet of the mouse tricuspid valve leaflet has not yet delaminated at birth.

Venous Structures and Atrial Appendages

Bilateral venae cavae (**Figure 5a**) and prominent atrial appendages (**Figure 5c**) were seen in mature mouse fetuses; in human

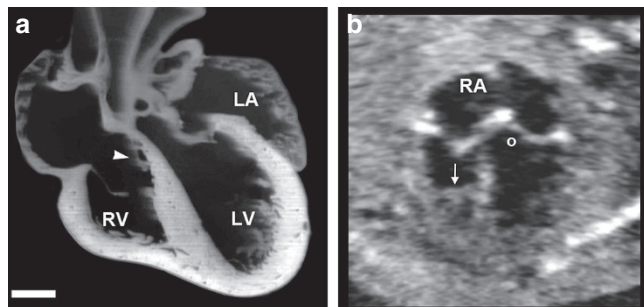


Figure 4. Morphologic characteristics of right versus left ventricle. (a) Mouse heart in frontal plane section immediately at term birth. Scale bar = 400 μ m. Note the tricuspid valve septal leaflet (arrowhead) has not delaminated from the ventricular septum. The tricuspid valve annulus sits inferior to the mitral valve annulus, similar to that in the human. (b) A fetal echocardiographic image from a human fetus in the second trimester. RA, right atrium. An arrow indicates the presence of a moderator band. The "o" symbol indicates the atrioventricular septum or area of offset between the mitral and tricuspid valve.

fetuses, atrial appendages were small (**Figure 5f**), and a single right superior vena cava was present (**Figure 5d**). In contrast to the human with multiple pulmonary vein orifices (**Figure 5e**), a pulmonary venous confluence with one orifice enters the left atrium in mice (**Figure 5b**).

Atrioventricular Valve Morphogenesis

The development of the atrioventricular valves is seen over E10.5–E17.5 in the mouse and CS 16–23 (EGA 7 3/7–9 3/7 wk) in the human. During the looped heart tube stage, large endocardial cushions were present (**Figure 6a** mouse; **Figure 6c** human). The formation of a single atrioventricular junction was seen at 7 $\frac{3}{4}$ wk gestation (CS 16) in human (**Figure 6h**) and E11.5 in mouse (**Figure 6d**). By 8 wk gestation (CS 18; **Figure 6f**) in human and E12.5 (**Figure 6b**) in the mouse, separate right and left sided atrioventricular valves had developed. Note the thickened appearance of the valve leaflets. By CS 23 in the human, the valve leaflets had achieved a thin, mature appearance (**Figure 6g**). In the mouse, refinement of the atrioventricular valves and chordal apparatus continued until E17.5 (**Figure 6c**). Even at birth, tricuspid valve development in the mouse was not complete in that the septal leaflet of the tricuspid valve (**Figure 4**) remained adhered to the septum.

Outflow Septation

Outflow septation occurred during E11.5–E13.5 in the mouse and EGA 7 3/7–8 wk (CS 16–18) in the human (**Figure 7**). First, septation of the primitive outflow tract (**Figure 7a,e**)

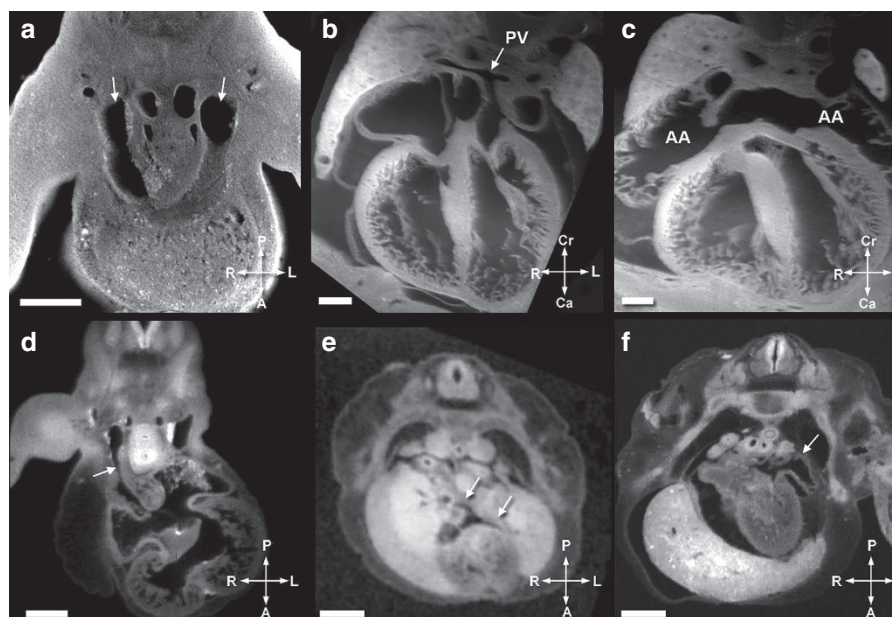


Figure 5. Comparative atrial and venous anatomy. (a–f) The comparative venous and atrial anatomy in the mouse and human. (a) Bilateral superior venae cavae are present in the mouse in contrast to (d) a single right superior vena cava in the human. The pulmonary veins in the human enter in (b) one orifice in the mouse in contrast to (e) separate orifices in the human. Atrial appendages are (c) large in mouse and (f) small in the human. (a) Mouse heart at E11.5. Scale bar = 400 μ m. Arrows indicate the bilateral superior venae cavae present in the mouse. (b) Mouse heart at E14.5. Scale bar = 350 μ m. "PV" and the arrow denote the single pulmonary vein orifice present in the mouse. (c) Mouse heart at E14.5. Scale bar = 350 μ m. AA, atrial appendages, which are large and constitute a significant portion of the mouse atria. (d) Human heart at EGA 7 3/7 wk (CS 16). Scale bar = 900 μ m. Arrow denotes the single right superior vena cava. (e) Human heart at EGA 8 wk (CS 18). Scale bar = 900 μ m. Arrows indicate the separate right and left pulmonary vein orifices. (f) Human heart at EGA 8 wk (CS 18). Scale bar = 900 μ m. Arrow indicates the atrial appendage which is small in the human in comparison to the mouse. CS, Carnegie stage; E, embryonic day; EGA, estimated gestational age.

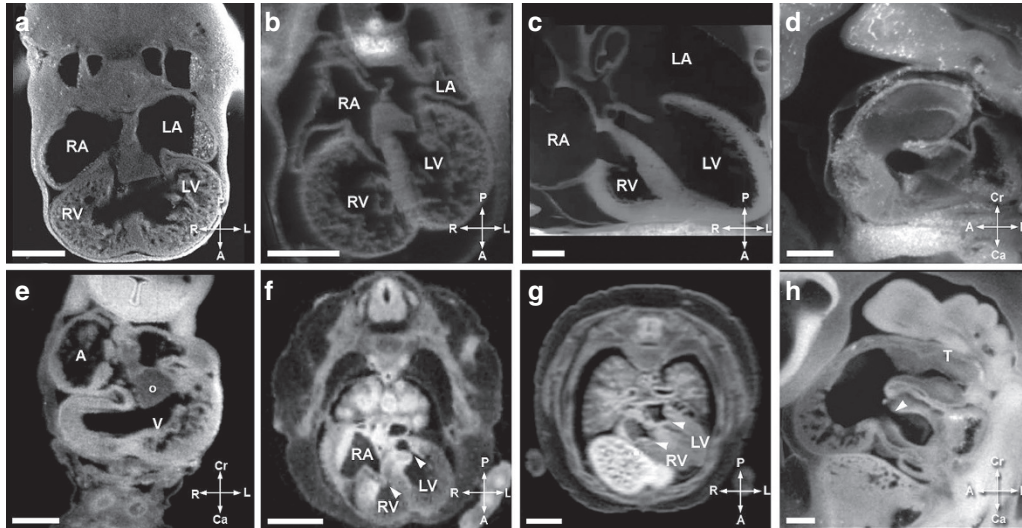


Figure 6. Comparative atrioventricular (AV) valve morphogenesis. (a–d) AV valve morphogenesis in the mouse. (e–h) AV valve morphogenesis in the human. Panels a and e show the mouse and human heart in the looped stage, with large endocardial cushion. Panels b (mouse) and f (human) show two distinct AV communications with thickened AV valves. The arrowheads in panels f, g, and h indicate the AV valve orifices as they develop. Panels c and g show the AV valves acquiring a thinner more mature appearance. Panel d shows a sagittal view of the AV junction at the looped heart stage of the mouse, and panel h highlights a similar figure in the human. (a) Mouse heart at E11.5. Scale bar = 400 μ m. LA, left atrium; LV, left ventricle; RA, right atrium; RV, right ventricle. (b) Mouse heart at E12.5. Scale bar = 550 μ m. (c) Mouse heart at E17.5. Scale bar = 400 μ m. (d) Mouse heart at E11.5. Scale bar = 400 μ m. (e) Human heart at EGA 6 6/7 wk (CS 14). Scale bar = 500 μ m. The “o” symbol indicates the inferior cushion. A, atrium; V, ventricle. (f) Human heart at EGA 8 wk (CS 18). Scale bar = 1,500 μ m. The arrowheads indicate the AV valve orifices. (g) Human heart at EGA 9 3/7 wk (CS 23). Scale bar = 2,000 μ m. The arrowheads indicate the AV valve orifices. (h) Human heart at EGA 7 3/7 wk (CS 16). Scale bar = 400 μ m. The arrowhead indicates the AV valve orifice. T, truncus arteriosus. Panels e–h are reprinted from ref. (16). Copyright 2009 American Heart Association. CS, Carnegie stage; E, embryonic day; EGA, estimated gestational age.

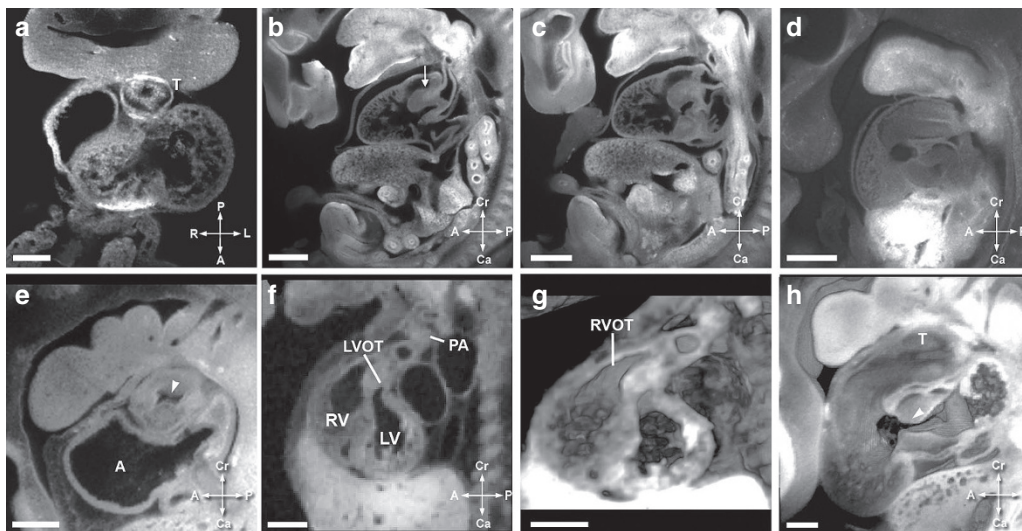


Figure 7. Comparative outflow tract septation. (a–d) Outflow tract septation in the murine heart. (e–h) Outflow tract septation in the human heart. Panels a (mouse) and e (human) show the outflow cushions in the unseptated outflow tract during the cardiac loop stage. (b–c) Distinct left and right ventricular outflow tracts in the mouse. (f,g) Distinct left and right ventricular outflow tracts in the human. Panel g is a 3-dimensional reconstruction of the image in f, and both are at EGA 8 wk (CS 18). At this stage in the mouse and human, the semilunar valve area is occupied by thick likely mesenchymal tissue, and discrete valve leaflets are not seen. Panel d shows a 3-dimensional reconstruction of the atrioventricular and outflow cushions in a mouse at stage E11.5, and panel h shows a comparable reconstruction in the human. The characteristic “dog leg bend” separating the proximal and distal outflow areas can be seen. The atrioventricular and outflow cushions are separate. In these images, the outflow cushions appear to be two long cushions, as opposed to separate proximal and distal cushions. (a) Mouse heart at E10.5. Scale bar = 135 μ m. T, truncus arteriosus. (b) Mouse heart at E12.5. Scale bar = 480 μ m. The arrow indicates the septation between the aortic and pulmonary outflow tracts. (c) Mouse heart at E12.5. Scale bar = 480 μ m. (d) Mouse heart at E11.5. Scale bar = 470 μ m. (e) Human heart at EGA 7 1/7 wk (CS 15). Scale bar = 630 μ m. The arrowhead shows unseptated lumen of the outflow. A, atrium. (f) Human heart at EGA 8 wk (CS 18). Scale bar = 1,350 μ m. LV, left ventricle; LVOT, left ventricular outflow tract; PA, pulmonary artery; RV, right ventricle. (g) Human heart at EGA 8 wk (CS 18). Scale bar = 1,350 μ m. RVOT, right ventricular outflow tract. (h) Human heart at EGA 7 3/7 wk (CS 16). Scale bar = 400 μ m. The arrowhead indicates the atrioventricular cushion. Panels e–h are reprinted from ref. (16). Copyright 2009 American Heart Association. CS, Carnegie stage; E, embryonic day; EGA, estimated gestational age.

into two separate arterial channels (**Figure 7b,c,f, and g**) occurs. Subsequently, semilunar valve morphogenesis takes place. Septation of the outflows begins with the formation of two mesenchymal ridges or cushions. These were seen at EGA 7¹/₇ wk (CS 15) in the human and were already noted at E9.5 in the mouse. Next, the ridges gradually spiral, eventually separating the distal outflow tract into the ascending aorta and pulmonary arteries. In our human specimens, at 7³/₇ wk (CS 16), and at E11.5 in the mouse, clockwise spiraling of the cushions is evident. The spiraling process in the human was shown in 2D imaging and 3D movies in previous work (16). At this stage, the outflow was a single channel proximally and a divided passageway with two separate channels distally.

By E12.5 in the mouse, two completely distinct outflow tracts, divided both proximally and distally were noted (**Figure 7b,c**). Thick plate-like valve structures were noted in the aortic and pulmonary positions. This corresponds to CS 18 (EGA 8 wk) in the human (**Figure 7f,g**). Valve leaflets have been proposed to originate from cavitations in the fused outflow cushions, with adjacent leaflets forming from cushions and facing leaflets forming from a second set of intercalated cushions (10). These intercalated cushions were not seen in either the mouse or human specimens in our study. During CS 18–23 (EGA 8–9 3/7 wk) in human and E12.5–E18.5 in the mouse, the semilunar valve leaflets undergo a process of thinning, acquiring the typical postnatal appearance.

Unique Characteristics of the Right and Left Ventricle

In the human, right vs. left ventricles can be distinguished by multiple factors. First, the tricuspid valve orifice sits inferior to the mitral valve. Second, the left ventricle has smooth trabeculations, while the right ventricle has coarse trabeculations. Third, the tricuspid valve has multiple chordal attachments to the ventricular septum, while the mitral valve does not. Finally, the right ventricle has a moderator band, while the left ventricle does not. These features are shown in a fetal echocardiogram from a second-trimester human fetus (**Figure 4b**).

In the mouse, we evaluated all specimens for these factors. As in the human, the tricuspid valve septal leaflet did have multiple chordal attachments to the septum, and the valve orifice was positioned inferiorly relative to the mitral valve. A moderator band could not be identified in the mouse right ventricle. These findings are illustrated by the specimen in **Figure 5b**. Two papillary muscles were seen in the left ventricle, similar to the human. No obvious differences in the trabeculations were noted by our imaging techniques, as previously described by Wessels and Sedmera (11).

DISCUSSION

Atrial and Ventricular Septation

Atrial septation was similar in both mouse and human. Our findings regarding the process of atrial septation were in agreement with the work by Anderson *et al.* (9). This process begins during the primary heart tube stage in both species. The principle structures involved in atrial septation were homologous and could be identified in both mouse and human.

We found ventricular septation to be similar in both the mouse and the human, although species-specific differences in ventricular septation have been described in the past. For example, in the chick embryo, the interventricular septum develops from compaction of multiple ventricular trabeculations (17), while in mammals, this is not seen. The final portion of the interventricular septum to close in both the mouse and human specimens comprised a portion of the membranous and inlet septum. This is a topic of controversy in cardiac development.

Outflow Septation

Outflow tract septation describes the process of transforming a single outflow tract from the right ventricle into divided pulmonary and aortic outflows originating from the right and left ventricles, respectively. It also includes the development of semilunar valve leaflets. This requires the development of ridges within the primitive outflow tract, fusion of these ridges, transformation of the ridges from myocardial tissue to arterial tissue, and development of valve leaflets. Cardiac neural crest cells migrate from the dorsal neural tube to the developing outflow tract; this process is necessary for normal septation. Cardiac neural crest cells are present in the outflow tract at approximately E9.5 in the mouse. Interestingly, differences occur between mammals and other species, such as the chick, in both the route of migration of the neural crest cells and the areas in the outflow tract where these cells are present (18).

Controversy exists as to the number of ridges, as well as to the appropriate terminology for the structures within the developing outflow tract (10,19–25). Species-specific differences exist in the nature of the outflow tract ridges. For example, in the chick, three distal ridges and two proximal ridges are present (25). In the human and mouse, it has been debated as to whether two long outflow ridges, or two proximal and two distal ridges in addition to two intercalated ridges are present. Webb *et al.* (25) and Anderson *et al.* (10) have described the initial outflow tract as having a “dog leg bend” which divides the proximal and distal outflows. The distal outflow is the area which clinicians refer to as the “truncus arteriosus” and the proximal outflow gives rise to the valve leaflets and sinuses.

No major differences in outflow tract septation between mouse and human species were identified in this study. The processes of spiraling, fusion with endocardial cushions, and thinning of plate-like structures to form semilunar valves were comparable. In our study, two ridges were identified in the outflow tract of the mouse and human and intercalated ridges were not seen. Sophisticated molecular analysis studies in the human have also recently confirmed that the process of septation is similar in mice and human species, with formation of walls in the outflow tracts occurring by addition of ISL1-positive mesenchymal cells distally (26).

Distinction in Ventricular Morphology

Only some of the identifying characteristics between right and left ventricular morphology could be seen in the mouse. The ventricular morphology of the mouse is shown in **Figure 5b** and

was compared to a human fetal echocardiogram in **Figure 4b**. Specifically, offset between the tricuspid and mitral valves was noted. Additionally, tricuspid valve chordal attachments to the septum were seen. The septal leaflet was not delaminated even immediately after birth, corroborating findings by others (27,28). Interestingly, a moderator band could not be identified in the mouse right ventricle, and a difference in trabeculations was not noted. This confirms prior work (27). Differences may exist at the microscopic level, beyond the scope of this study.

Time Course of Development

Within a few days after completion of cardiac morphogenesis, mice are born, but in humans, several months of gestation remain. This may allow emergence of cardiac defects in humans not seen in mice due to hemodynamic remodeling. Specifically, we believe that mouse modeling of some forms of hypoplastic left heart syndrome, progressive pulmonic stenosis, and Ebstein's anomaly may be temporally different than that in the human fetus. Interestingly, in a study of the first 10,000 *N*-ethyl-*N*-nitrosourea mutagenized mouse fetuses, hypoplastic left heart syndrome and Ebstein's anomaly were not identified, although almost all other major cardiac defects were seen (29). In a subsequent 10,000 studied fetuses, hypoplastic left heart syndrome has rarely been identified (30). Hypoplastic left heart syndrome is a heterogeneous disease in the human, with a subset of fetuses who initially have aortic stenosis that progresses throughout the second and third trimester (31). It is possible that only certain types of hypoplastic left heart syndrome can be replicated in mouse models.

Conclusions

The sequence of cardiac development in the mouse and human is similar. We lay out these parallel sequences both with description and images in this manuscript. Comprehensive, high-resolution atlases with 3D volumes were used for the study and are provided as a resource for clinicians and scientists studying normal and diseased cardiac development.

METHODS

EFIC Imaging of Mouse Embryos

This animal study protocol was approved by the Animal Care and Use Committee of the National Heart, Lung, and Blood Institute, National Institutes of Health, Bethesda, MD. We processed and imaged inbred and outbred mouse strains using EFIC (Charles River Laboratories, Wilmington, MA). Mouse embryos between stages E9.5 and birth were examined, with E0.5 being defined as identification of conception plug. We have previously described the EFIC method (14,15). EFIC is a technique which takes advantage of the natural fluorescence of pyridine nucleotides present within all cells. This fluorescent signal can be preserved by formaldehyde. Embryonic specimens are embedded in wax containing aniline Sudan IV dye. The embedded embryo's block face is serially imaged after each cut. Imaging on the block face eliminates 2D registration errors; additionally, processing software allows the stacked images to be rotated into different viewing planes and resectioned.

A portion of human and mouse embryos studied were previously compiled into digital atlases (website manufacture: National Heart Lung and Blood Institute, Bethesda, MD; database and software: Microsoft SQL and Asp.net application in C# ("c sharp"), Redmond, WA). These images and volumes were also reviewed for the purposes

of this study. The mouse atlas can be accessed at: <http://apps.devbio.pitt.edu/MouseAtlas>. The human atlas can be accessed at: <http://apps.devbio.pitt.edu/HumanAtlas>. The username is "Human" and password is "Embryo." Detailed instructions for these atlases are available online after logging in.

Embryos were harvested and fixed with 10% formalin. Embryos were dehydrated using serial exposure to 70, 95, and 100% alcohol with differing incubation times according to the age of the embryo. We soaked the embryos 2–3 times in xylene for 15 min each, followed by an ~5 h soak in 70.4% paraffin wax (containing 24.9% Vybar, 4.4% stearic acid, and 0.4% aniline dye Sudan IV). The paraffin wax was changed twice during the incubation, once every 30 min and then incubated for 4 h without disturbance. The wax changes eradicated any residual alcohol or xylene. Following this, we embedded embryos in a metal mold filled with 70.4% paraffin wax and cooled for 1 h at 21 °C.

Sectioning was done using a Leica SM2500 microtome mounted with a MZFLIII stereomicroscope equipped with a mercury lamp and Hamamatsu Orca ER CCD camera with excitation/emission filters of 425/480 nm, respectively (Leica Microsystems, Bannockburn, IL; Hamamatsu, Bridgewater, NJ). Four to 5 µm sections were imaged and captured using Open Lab 3.5 software (Improvision, Waltham, MA).

Volocity (Improvision) and Open Lab 3.5 software (Improvision) were used for viewing images. We studied stacks in deviated transverse and sagittal planes for visualization of key developmental events, and when necessary rotated into off axis views using Volocity.

EFIC and MRI Imaging of Human Embryos

Using MRI and EFIC, we examined 52 human embryos from 6 4/7–9 3/7 wk gestation as described in previous work (16). EFIC techniques were similar to those described for the mouse. MRI images were obtained using a 7.0T Bruker vertical bore MRI with 150 G/cm gradients and 5–30 mm birdcage coils or 7.0T 16 mm horizontal bore Bruker Paravision system with 39 G/cm gradient and 38 mm birdcage coil. Samples were imaged using 3D rapid gradient echo (SNAP) sequence using repetition time 30–40 ms, echo time 3.3–4 ms, 20–90 averages, acquisition time 12–50 h.

Comparison of Mouse and Human Morphogenesis

We systematically reviewed each specimen to identify whether specific anatomic characteristics of atrioventricular and outflow septation, valve formation, venous morphology, and ventricular structure could be identified at each stage. Prior to evaluation, the image quality of each specimen was noted.

SUPPLEMENTARY MATERIAL

Supplementary material is linked to the online version of the paper at <http://www.nature.com/pr>

ACKNOWLEDGMENTS

We thank Srujan Boppana for his technical assistance with creation and use of the human and mouse atlases. We also thank Dr Subbu Subramaniam for his pathology expertise in reviewing the specimens.

STATEMENT OF FINANCIAL SUPPORT

This work was supported by United States National Institutes of Health grant ZO1-HL005701. The Kyoto collection was supported by the Japanese Ministry of Education, Culture, Sports, Science, and Technology (grant 19390050); Japanese Ministry of Health, Labor, and Welfare (grant 17A-6); and Japan Science Technology Agency (BIRD grant). S.Y. was supported by Kyoto University Foundation. L.L. had a subgrant from the intramural Center of Genetics and Developmental Biology, National Heart Lung and Blood Institute, National Institutes of Health, Bethesda, MD.

Disclosure: None.

REFERENCES

1. Mitchell SC, Korones SB, Berendes HW. Congenital heart disease in 56,109 births. Incidence and natural history. *Circulation* 1971;43:323–32.
2. DeLaughter DM, Saint-Jean L, Baldwin HS, Barnett JV. What chick and mouse models have taught us about the role of the endocardium in congenital heart disease. *Birth Defects Res A Clin Mol Teratol* 2011;91:511–25.

3. MacGrogan D, Nus M, de la Pompa JL. Notch signaling in cardiac development and disease. *Curr Top Dev Biol* 2010;92:333–65.
4. Webb S, Brown NA, Anderson RH. Formation of the atrioventricular septal structures in the normal mouse. *Circ Res* 1998;82:645–56.
5. Nishimura H, Takano K, Tanimura T, Yasuda M. Normal and abnormal development of human embryos: first report of the analysis of 1,213 intact embryos. *Teratology* 1968;1:281–90.
6. Vuillemin M, Pexieder T. Normal stages of cardiac organogenesis in the mouse: I. Development of the external shape of the heart. *Am J Anat* 1989;184:101–13.
7. Vuillemin M, Pexieder T. Normal stages of cardiac organogenesis in the mouse: II. Development of the internal relief of the heart. *Am J Anat* 1989;184:114–28.
8. Moorman A, Webb S, Brown NA, Lamers W, Anderson RH. Development of the heart: (1) formation of the cardiac chambers and arterial trunks. *Heart* 2003;89:806–14.
9. Anderson RH, Webb S, Brown NA, Lamers W, Moorman A. Development of the heart: (2) Septation of the atriums and ventricles. *Heart* 2003;89:949–58.
10. Anderson RH, Webb S, Brown NA, Lamers W, Moorman A. Development of the heart: (3) formation of the ventricular outflow tracts, arterial valves, and intrapericardial arterial trunks. *Heart* 2003;89:1110–8.
11. Wessels A, Sedmera D. Developmental anatomy of the heart: a tale of mice and man. *Physiol Genomics* 2003;15:165–76.
12. Sissman NJ. Developmental landmarks in cardiac morphogenesis: comparative chronology. *Am J Cardiol* 1970;25:141–8.
13. Sedmera D. Function and form in the developing cardiovascular system. *Cardiovasc Res* 2011;91:252–9.
14. Rosenthal J, Mangal V, Walker D, Bennett M, Mohun TJ, Lo CW. Rapid high resolution three dimensional reconstruction of embryos with episcopic fluorescence image capture. *Birth Defects Res C Embryo Today* 2004;72:213–23.
15. Weninger WJ, Mohun T. Phenotyping transgenic embryos: a rapid 3-D screening method based on episcopic fluorescence image capturing. *Nat Genet* 2002;30:59–65.
16. Dhanantwari P, Lee E, Krishnan A, Samtani R, et al. Human cardiac development in the first trimester: a high-resolution magnetic resonance imaging and episcopic fluorescence image capture atlas. *Circulation* 2009;120:343–51.
17. Ben-Shachar G, Arcilla RA, Lucas RV, Manasek FJ. Ventricular trabeculations in the chick embryo heart and their contribution to ventricular and muscular septal development. *Circ Res* 1985;57:759–66.
18. Keyte A, Hutson MR. The neural crest in cardiac congenital anomalies. *Differentiation* 2012;84:25–40.
19. Bajolle F, Zaffran S, Meilhac SM, Dandonneau M, et al. Myocardium at the base of the aorta and pulmonary trunk is prefigured in the outflow tract of the heart and in subdomains of the second heart field. *Dev Biol* 2008;313:25–34.
20. Bartelings MM, Gittenberger-de Groot AC. The outflow tract of the heart—embryologic and morphologic correlations. *Int J Cardiol* 1989;22:289–300.
21. Kramer T. The partitioning of the truncus and conus and the formation of the membranous portion of the interventricular septum in the human heart. *Am J Anat* 1942;71:343–70.
22. Orts-Llorca F, Puerta Fonolla J, Sobrado J. The formation, septation and fate of the truncus arteriosus in man. *J Anat* 1982;134(Pt 1):41–56.
23. Restivo A, Piacentini G, Placidi S, Saffirio C, Marino B. Cardiac outflow tract: a review of some embryogenetic aspects of the conotruncal region of the heart. *Anat Rec A Discov Mol Cell Evol Biol* 2006;288:936–43.
24. Tonge M. Observations on the development of the semilunar valves of the aorta and pulmonary artery of the heart of the chick. *Phil Trans Roy Soc (London)* 1869;159:387–411.
25. Webb S, Qayyum SR, Anderson RH, Lamers WH, Richardson MK. Septation and separation within the outflow tract of the developing heart. *J Anat* 2003;202:327–42.
26. Sizarov A, Lamers WH, Mohun TJ, Brown NA, Anderson RH, Moorman AF. Three-dimensional and molecular analysis of the arterial pole of the developing human heart. *J Anat* 2012;220:336–49.
27. Webb S, Brown NA, Anderson RH. The structure of the mouse heart in late fetal stages. *Anat Embryol (Berl)* 1996;194:37–47.
28. Shakibi JG, Diehl AM. Postnatal development of the heart in normal Swiss-Webster mice. *Lab Anim Sci* 1972;22:668–83.
29. Shen Y, Leatherbury L, Rosenthal J, Yu Q, et al. Cardiovascular phenotyping of fetal mice by noninvasive high-frequency ultrasound facilitates recovery of ENU-induced mutations causing congenital cardiac and extra-cardiac defects. *Physiol Genomics* 2005;24:23–36.
30. Liu X, Saeed S, Li Y, et al. Abstract 19570: a multigenic etiology of hypoplastic left heart syndrome: an analysis based on three novel mutant mouse models of hypoplastic left heart syndrome. *Circulation* 2012;126:A19570.
31. McElhinney DB, Marshall AC, Wilkins-Haug LE, Brown DW, et al. Predictors of technical success and postnatal biventricular outcome after in utero aortic valvuloplasty for aortic stenosis with evolving hypoplastic left heart syndrome. *Circulation* 2009;120:1482–90.